IJCTA, 10(03), 2017, pp. 195-209

Analysis of Broken Bar Fault of Three Phase Induction Motor using Wavelet and Park's Vector Techniques

K. Mohanraj* Subhransu Sekhar Dash* V. Kalyanasundaram* and S. Paramasivam**

Abstract : The ultimate objective of this work is to model the three phase induction motor under healthy and broken rotor bar fault condition, and investigate the broken bar faults using wavelet technique and Park's vector approach. For analyzing the broken bar fault of the induction motor, wavelet technique and Park's vector approach are used. Wavelet is a mathematical tool that diagnoses the broken bar fault accurately with any one phase current. In the Park's vector technique, three phase currents are converted into direct axis and quadrature axis currents, and using these two currents broken rotor bar faults are diagnosed. Induction motor current is taken and analyzed for the healthy, one bar broken and two bars broken state of the induction motor. Wavelet co-efficients magnitude increases as the number of broken bars increase. Park's vector pattern for the faulty condition of the induction motor is quite different from the healthy condition of the induction motor. This diagnosis is used in the industries where motor is subjected to high stress. Diagnosis of the broken bar fault can also be done using the soft computing techniques.
Keywords: Broken bar, Induction motor, Wavelet, Park's vector approach, Diagnosis.

Nomenclature

L_s	Stator inductance
L_m	Mutual inductance
L_r	Rotor inductance
R_s	Stator resistance
R_r	Rotor resistance
ω_r	Rotor speed
P	Pole number
V_a, V_b, V_c	Stator three phase voltage
V_{ds}, V_{qs}	*d*-axis and *q*-axis components of the stator voltage vector V_s
V_{dr}, V_{qr}	*d*-axis and *q*-axis components of the rotor voltage vector V_r
i_a, i_b, i_c	Stator three phase currents
i_{ds}, i_{qs}	*d*-axis and *q*-axis components of the stator current vectors is
i_{dr}, i_{qr}	d-axis and q-axis components of the rotor current vectors ir
J	Moment of inertia of rotor
J_L	Moment of inertia of load
T_l	Load torque
T_e	Electromagnetic torque
P	Operator *d*/*dt*

* Assistant Professor, Professor, Assistant Professor, Electrical and electronics Department, Srm University, Kattankulathur 603203, India. *E-mail : mohanraajkumar@gmail.com, munu_dash_2k@yahoo.com, kalyan.srm@gmail.com*

** Manager, R & D, ESAB, Chennai. *E-mail : paramsathya@yahoo.com*

1. INTRODUCTION

Induction motors are reliable and most widely used motors in the industries as they require less maintenance. In general, fault diagnosis of induction motors has concentrated on sensing failures in one of three major components the stator, the rotor, and the bearings. Rotor faults have same frequency as the fundamental frequency of the motor.

Even though mechanical sensing techniques based on thermal and vibration monitoring have been utilized widely, most of the recent research has been directed toward electrical sensing with emphasis on analyzing the motor stator current. Rotor asymmetries are detected through the presence of sideband components around the fundamental component. However, some load torque oscillations or mechanical load abnormalities may produce similar effects in the current spectrum (*i.e.*, sidebands at similar frequencies), making the rotor fault diagnosis difficult [1-5]. Rotor broken bar can also be found from the Park's vector pattern, and wavelet detail co-efficient obtained for the broken bar fault signal obtained from the induction motor stator current [6-10].

An induction machine is a highly symmetrical electromagnetic system. Any fault will induce a certain degree of asymmetry[11-16]. Broken bars in induction machines can cause the asymmetry of the resistance and inductance in rotor phases, and consequently the asymmetry of the rotating electromagnetic field in the air gap, which will eventually induce frequency harmonics in stator current. Therefore, the broken bar impact can be modeled by unbalancing the rotor resistance and inductance [17-21].

2. MODELING OF INDUCTION MOTOR

Induction motor is modeled using the following equations in Matlab / Simulink.

A. Supply Voltage

$$V_a = V\sin(\omega t + \theta) \tag{1}$$

$$V_b = V\sin\left(\omega t - \frac{2\pi}{3} + \theta\right) \tag{2}$$

$$V_c = V\sin\left(\omega t - \frac{4\pi}{3} + \theta\right) \tag{3}$$

Three phase supply voltage is given by the equations V_a, V_b and V_c. Phase '*a*' voltage (V_a) is taken as the reference, phase '*b*' voltage (V_b) is 120 degree lagging the V_a, and phase '*c*' voltage (V_c) is 240 degree lagging the V_a.

B. Voltage Equations from Three Phases to Two Axes

Three phase voltage equations are converted into two voltage axes, direct axis voltage and quadrature axis voltage quantities, by following equations 4 and 5.

$$V_{ds} = \frac{\sqrt{2}}{3}\left(V_a - \frac{1}{2}V_b - \frac{1}{2}V_c\right) \tag{4}$$

$$V_{qs} = \frac{\sqrt{2}}{3}\left(\frac{\sqrt{3}}{2}V_b - \frac{\sqrt{3}}{2}V_c\right) \tag{5}$$

C. Primitive Voltage Equations of Three Phase Induction Motor

Primitive voltage. *e* equations of three phase induction motor model are given below between equations 6 and 9.

$$V_{ds} = R_{ds}I_{ds} + L_{ds}I_{ds}P + L_{md}PI_{dr} \quad (6)$$

$$V_{qs} = R_{qs}I_{qs} + L_{qs}I_{qs}P + L_{mq}PI_{qr} \quad (7)$$

$$V_{dr} = L_{md}I_{ds}P - L_{mq}\,\omega_r I_{qs} + R_{dr}I_{dr} + L_{dr}I_{dr}P - L_{qr}\omega_r I_{qr} \quad (8)$$

$$V_{qr} = L_{mq}I_{qs}P - L_{md}\,\omega_r I_{ds} + R_{qr}I_{qr} + L_{dr}I_{dr}\,\omega_r - L_{qr}I_{qr}P \quad (9)$$

D. Equations for Electrical Model

Electrical model of the induction motor is shown in Figure 1. Electrical model of the induction motor can be obtained by using the equations from 10 to 14.

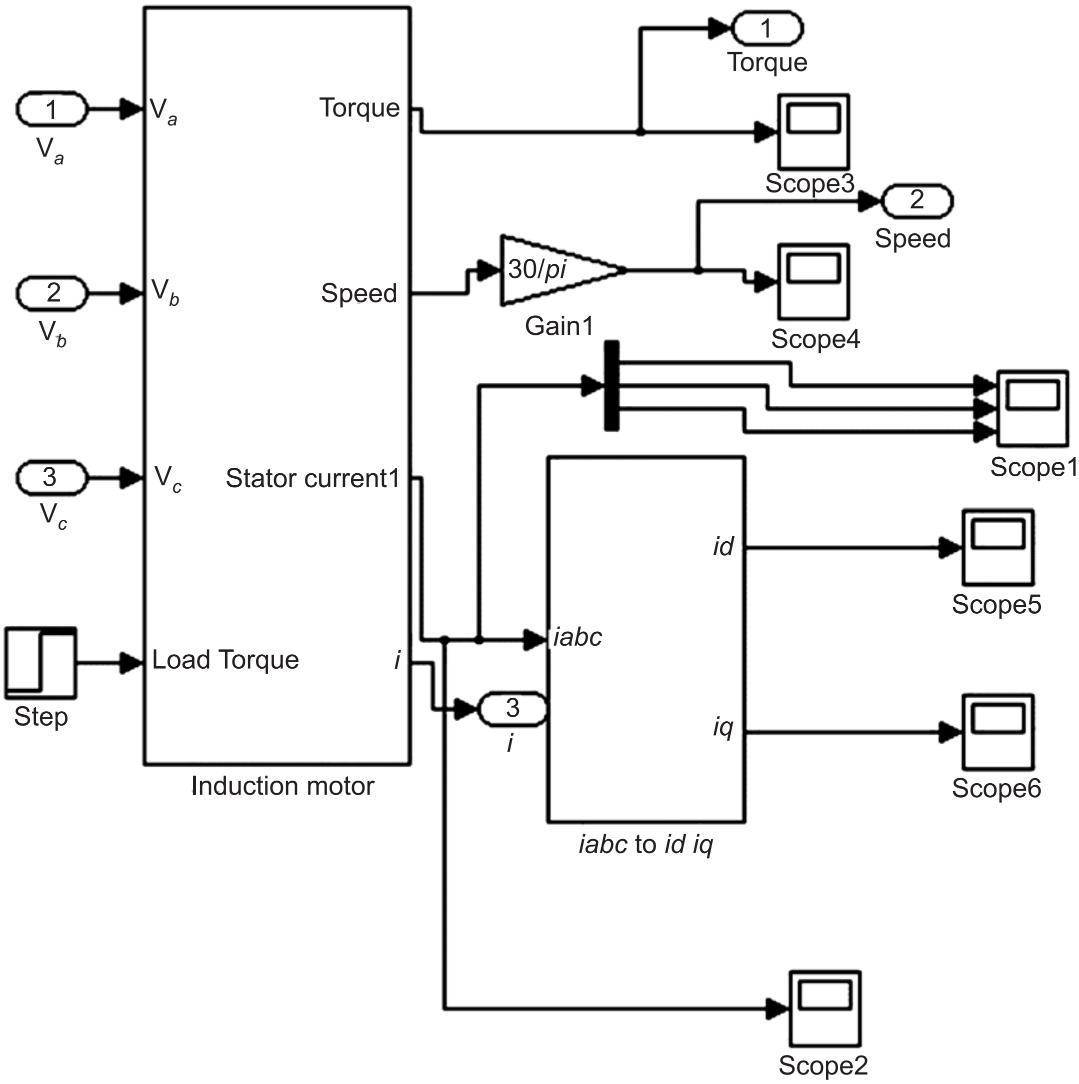

Figure 1: Electrical model

Induced emf,

$$e = L\frac{di}{dt} \quad (10)$$

$$e\frac{1}{L} = \frac{di}{dt} \quad (11)$$

$$\int e\frac{1}{L} = i(t) \quad (12)$$

$$i(t) = \frac{1}{L}\int e \quad (13)$$

$$i(t) = \frac{1}{L}\int (V - Ri) \tag{14}$$

E. Torque and Mechanical model

Electromagnetic torque of the induction motor model can be obtained by using the equations 15 and 16.

$$T_e = [I_{qr}[L_{dr}I_{dr} + M_d I_{ds}] - I_{dr}[L_{qr}I_{qr} + M_q I_{qs}]] \tag{15}$$

$$T_e = [I_{qr}\varphi_{dr} - I_{dr}\varphi_{qr}] \tag{16}$$

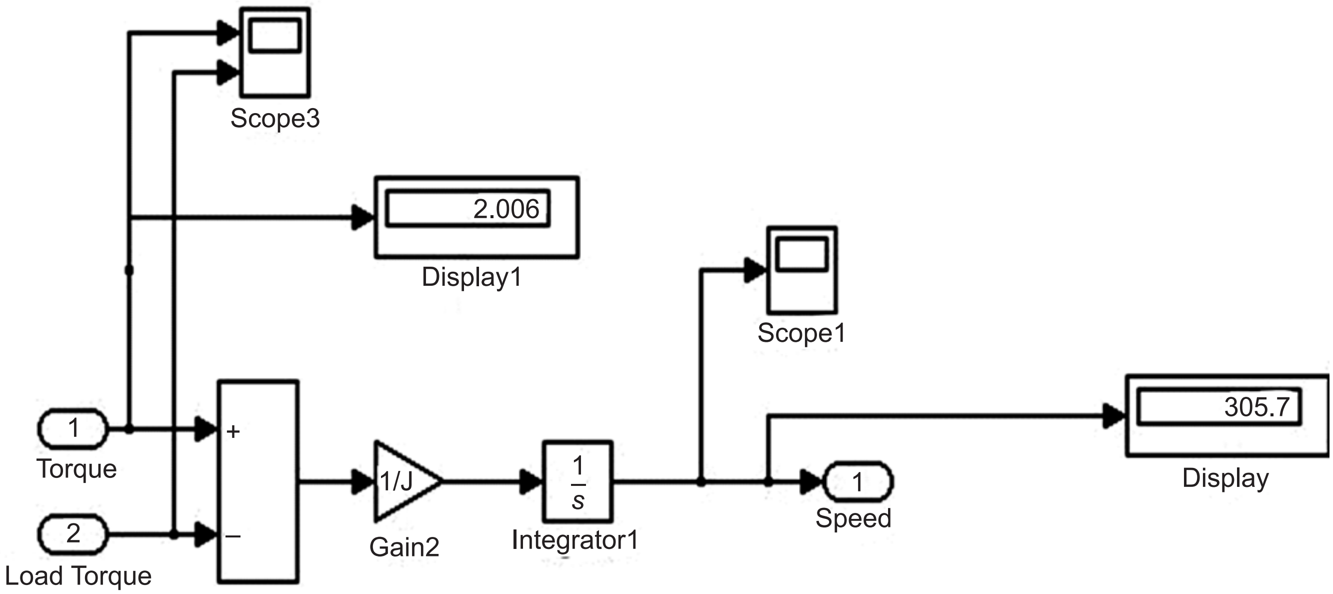

Figure 2: Relationship between torque and speed

Relationship between torque and speed is as follows.

$$T_e = J\frac{d^2\theta}{dt^2} + B\frac{d\theta}{dt} + K + T_l \tag{17}$$

$$T_e - T_1 = J\frac{d^2\theta}{dt^2} + B\frac{d\theta}{dt} \tag{18}$$

$$T_e - T_1 = JS\,\omega_r + B\omega_r \tag{19}$$

$$T_e - T_1 = [JS\,\omega_r + B]\omega_r \tag{20}$$

$$\frac{T_e - T_l}{[JS + B]} = \omega_r \tag{21}$$

$$\frac{T_e - T_l}{[JS]} = \omega_r \tag{22}$$

3. MODELING OF INDUCTION MOTOR ROTOR BAR FAULT

All the rotor bars will have same resistance and inductance values. Then rotor resistance, R_r, can be taken as number of rotor bars multiplied by the resistance of each bar. Similarly, the rotor inductance, L_r, can be calculated from number of rotor bars multiplied by the inductance of each bar. Relationship between torque and speed is shown in Figure 2. Induction motor with supply is shown in Figure 3.

$$R_r = N.r_r \tag{23}$$

$$L_r = N.1_r \tag{24}$$

Where,

N Number of rotor bars

r_r Rotor resistance of each rotor bar

l_r Rotor inductance of each rotor bar

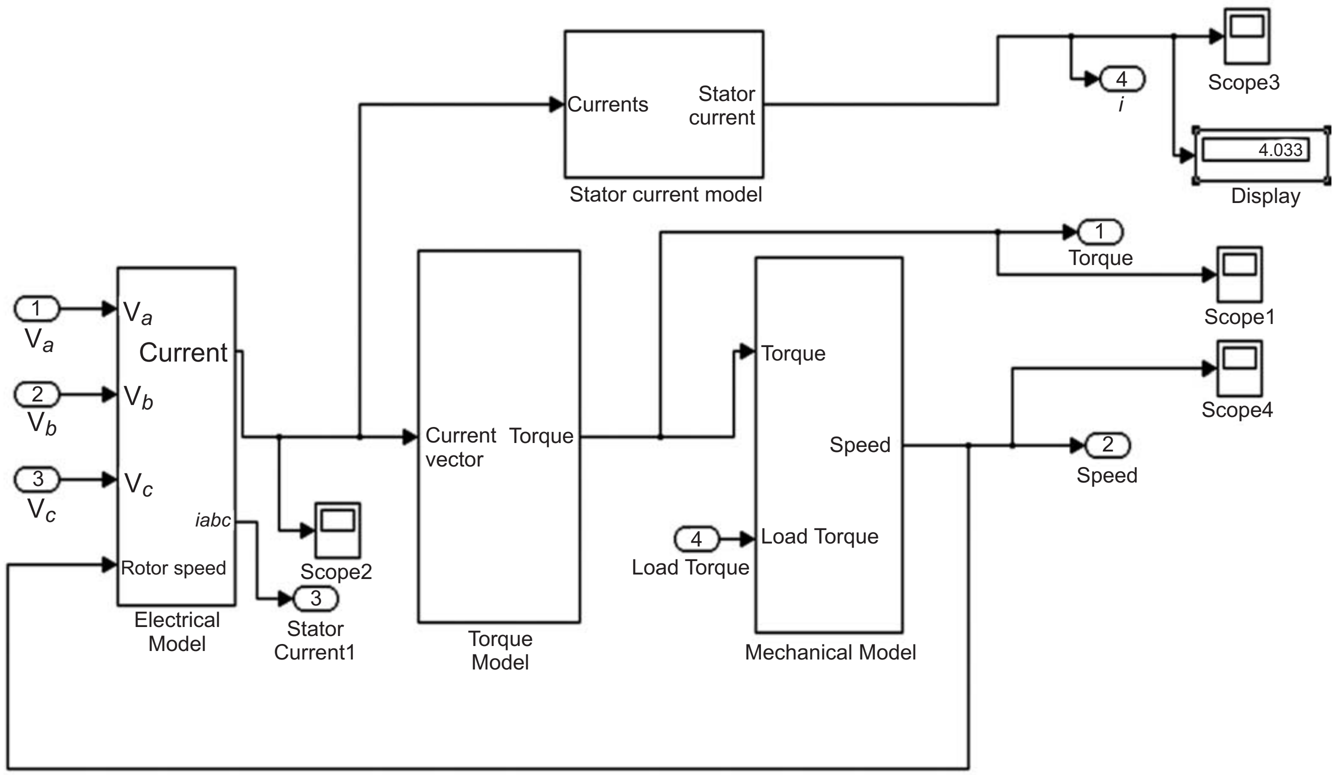

Figure 3: Induction motor with supply

One bar broken fault is created by reducing the value of resistance and inductance corresponding to one rotor bar in the resistance and inductance matrix respectively, and similarly the two broken bar fault is created by reducing the value of resistance and inductance corresponding to two rotor bars in the resistance and inductance matrix of the induction motor model respectively.

4. BROKEN BAR FAULT DIAGNOSIS TECHNIQUES

A. Wavelet Analysis

The main advantage of wavelet analysis over Fourier analysis is that it does not require time function involved to be periodic. This means that wavelet could be applied for transient analysis and faults detection because, in this case, the stator current is generally not a periodic function of time. Wavelets are well-suited for approximating data with sharp discontinuities.

Wavelet decomposition results in useful data that has '*details*' and '*approximate*' parts The '*approximation*' signal can further be decomposed into a new set of '*approximation*' and '*details*' signals and continue until *n* decomposition levels. The '*details*' signal contains high frequency information whereas the approximate part contains signal data with the low frequency components. Computing this decomposition to *n* levels results in those higher detail parts being removed, thereby reducing the overall frequency characteristics of the resulting data. This implies that lower levels of decomposition provide detail data that contains the highest frequency components. This high frequency components obtained provides the status of the induction motor [9-10].

For finding the broken rotor bar fault, motor current signal is analyzed with respect to six 'details' level. In this simulation, daudechies wavelet is used to analyze the current signal.

Ripples in the sixth 'detail' level clearly indicates how well the performance of the induction motor deviates from healthy condition during one broken bar and two broken bar of the induction motor.

B. Current Park's Vector Approach

Three phase stator currents I_a, I_b and I_c in amperes are computed and then current Park's vector pattern is determined on the basis of three to two phases transformation model.

Park's vector components (I_d, I_q) are :

$$I_d = \sqrt{\frac{2}{3}}\, I_a - \sqrt{\frac{1}{6}}\, I_b - \sqrt{\frac{1}{6}}\, I_c \tag{25}$$

$$I_q = \sqrt{\frac{1}{2}}\, I_b - \sqrt{\frac{1}{2}}\, I_c \tag{26}$$

Pattern obtained from the I_d and I_q currents is almost circular in nature for the healthy induction motor and the patterns obtained from the park's vectors I_d and I_q for the broken bars are not exactly circular as the values of I_d and I_q changes[10]. From the variation in the values of I_d and I_q, it is understood that the severity of the fault due to the number of broken bars.

5. SIMULATION RESULTS

From the Figure 4 to Figure 6, it is observed that steady state currents for all the three motors are almost same but the transient currents are different *i.e.*, for healthy motor it is around 60 amps, for one bar broken it is around 80 amps, for two bar broken it is around 100 amps.

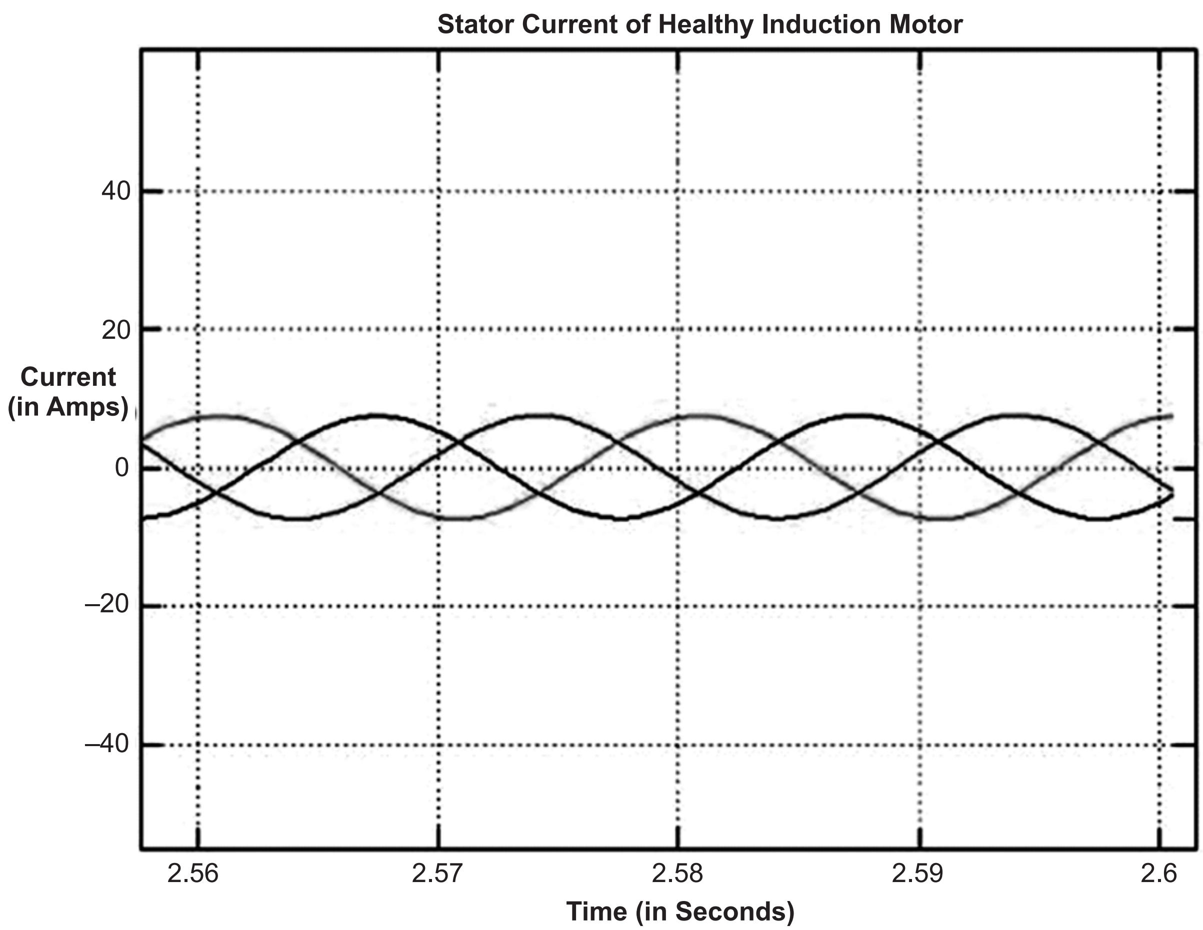

Figure 4: Healthy motor stator current of induction motor

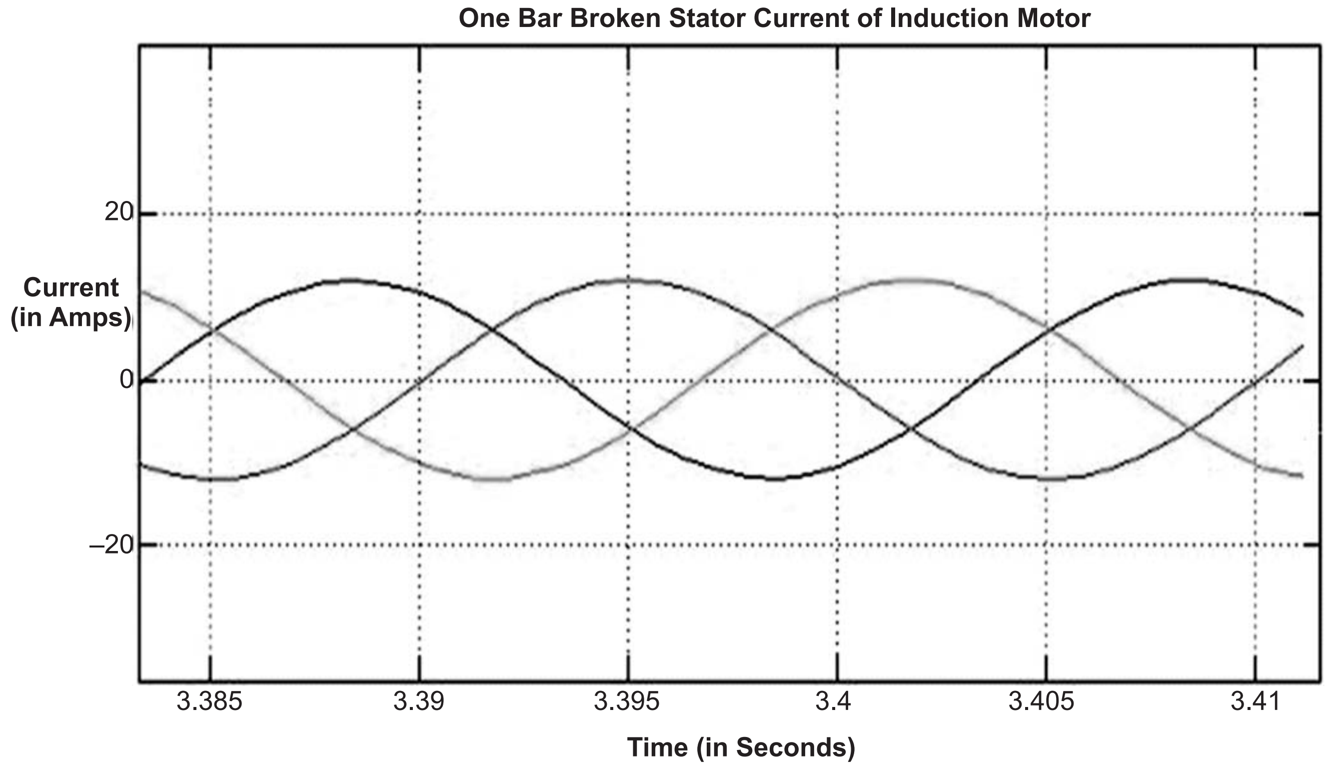

Figure 5: One bar broken stator current of induction motor

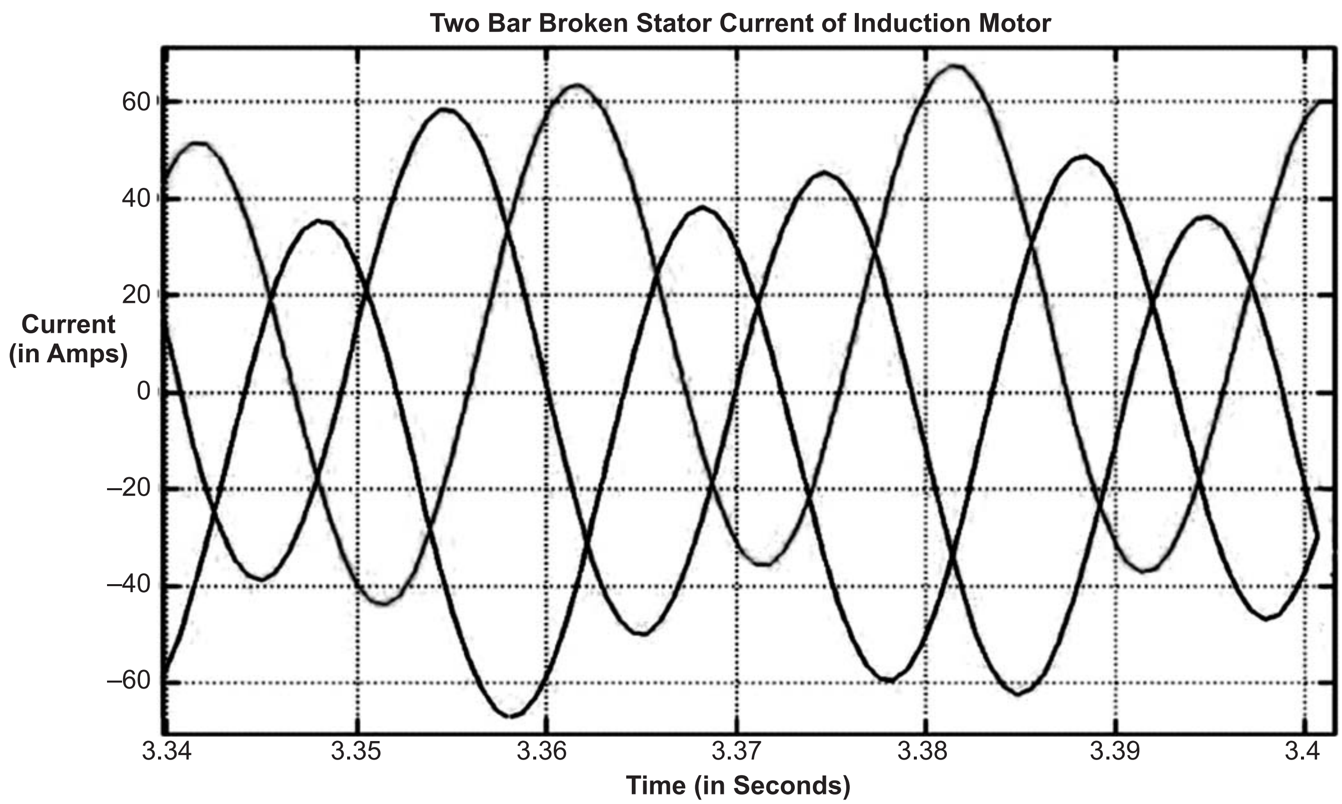

Figure 6: Two bar broken stator current of induction motor

In the induction motor, rotor bar breakage can be detected through motor current signature analysis. Mainly the effect will be on the transient condition of the motor and on the frequency side band components. On seeing the transient conditions in the healthy, one bar broken and two bar broken of the induction motor, it is clearly noted that the current has been increased in the fault conditions of the induction motor. These waveforms can be analysed clearly through wavelet technique.

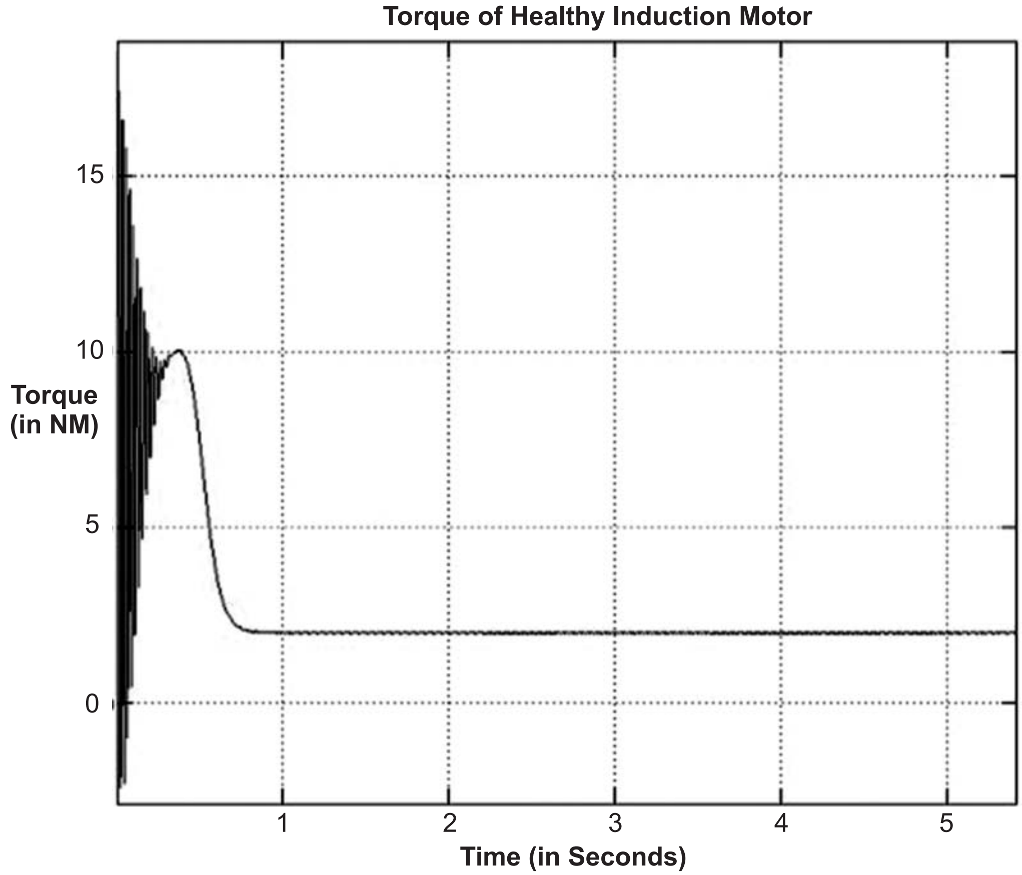

Figure 7: Torque of healthy induction motor

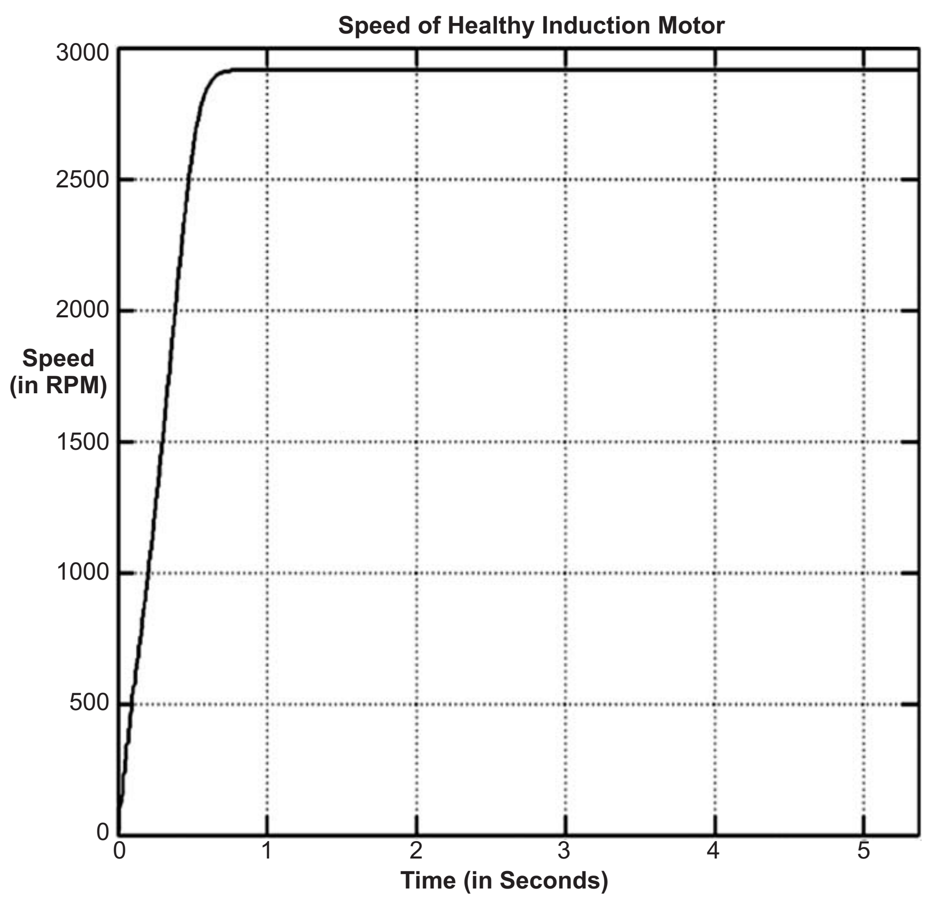

Figure 8: Speed of healthy induction motor

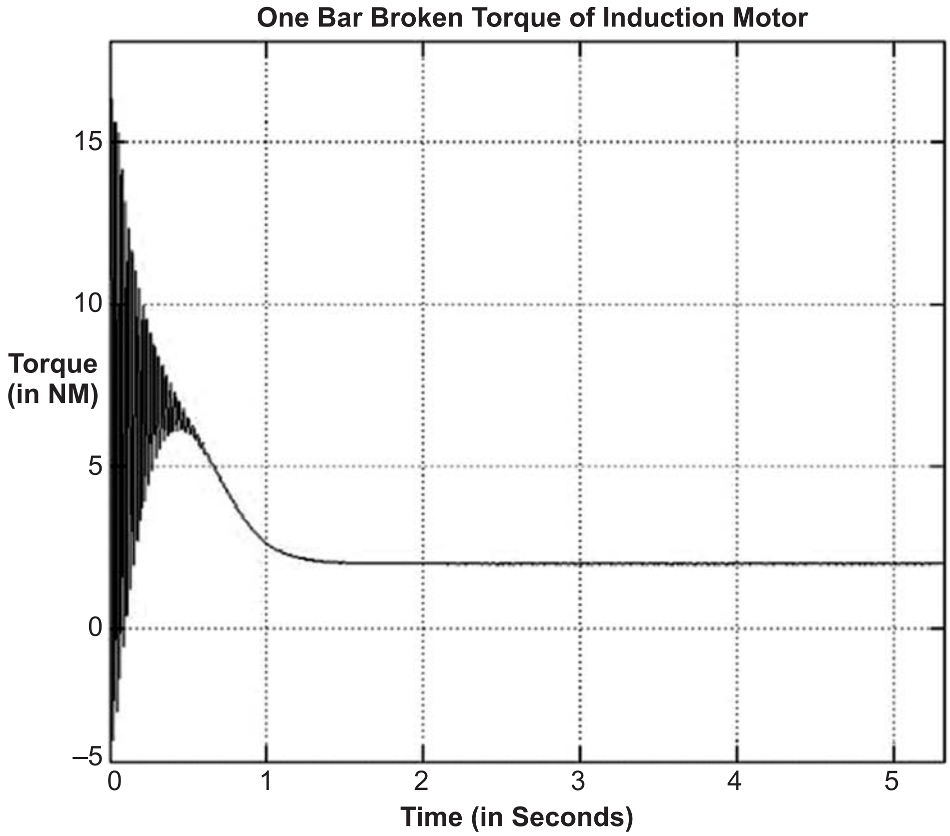

Figure 9: One bar broken torque of induction motor

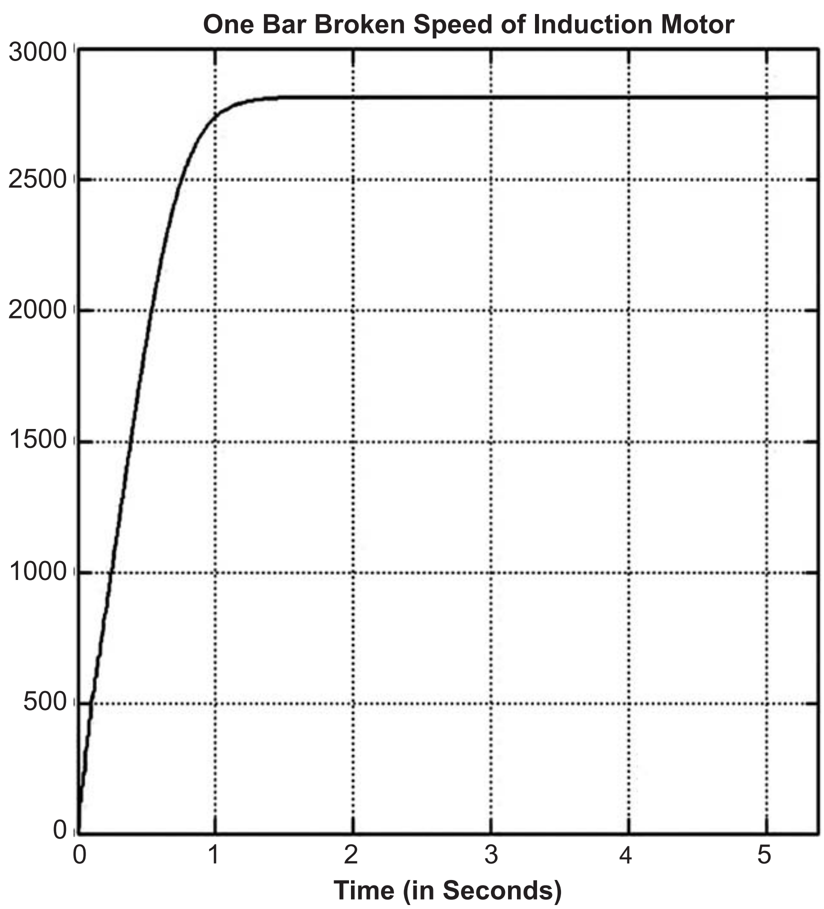

Figure 10: One bar broken speed of induction motor

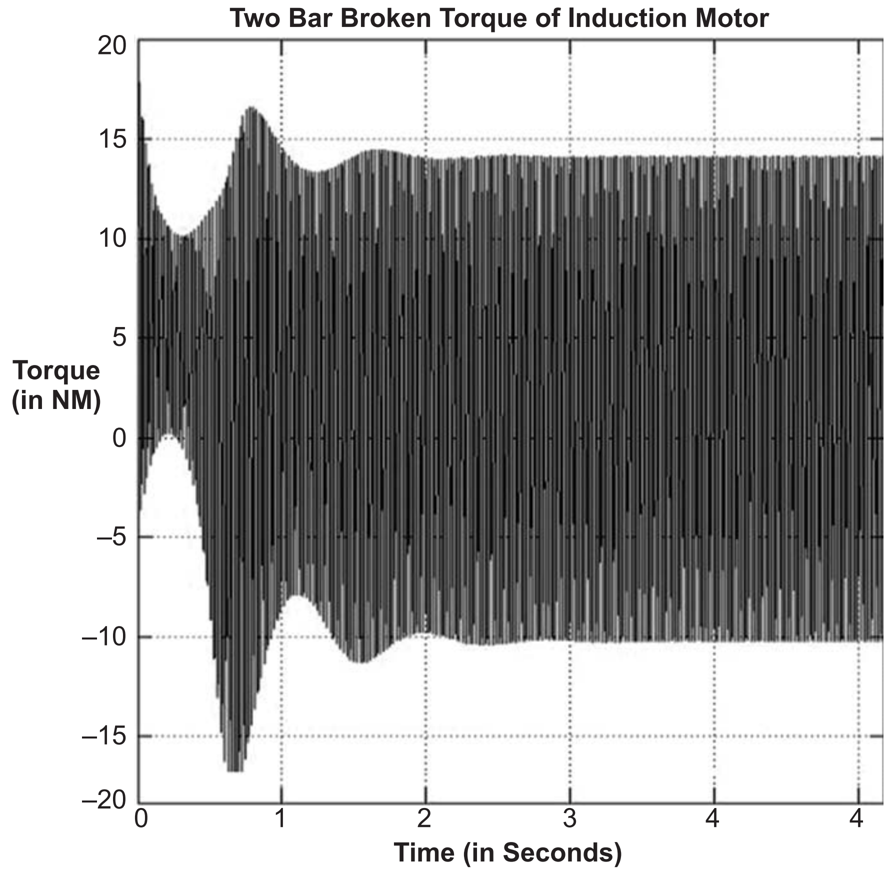

Figure 11: Two bar broken torque of induction motor

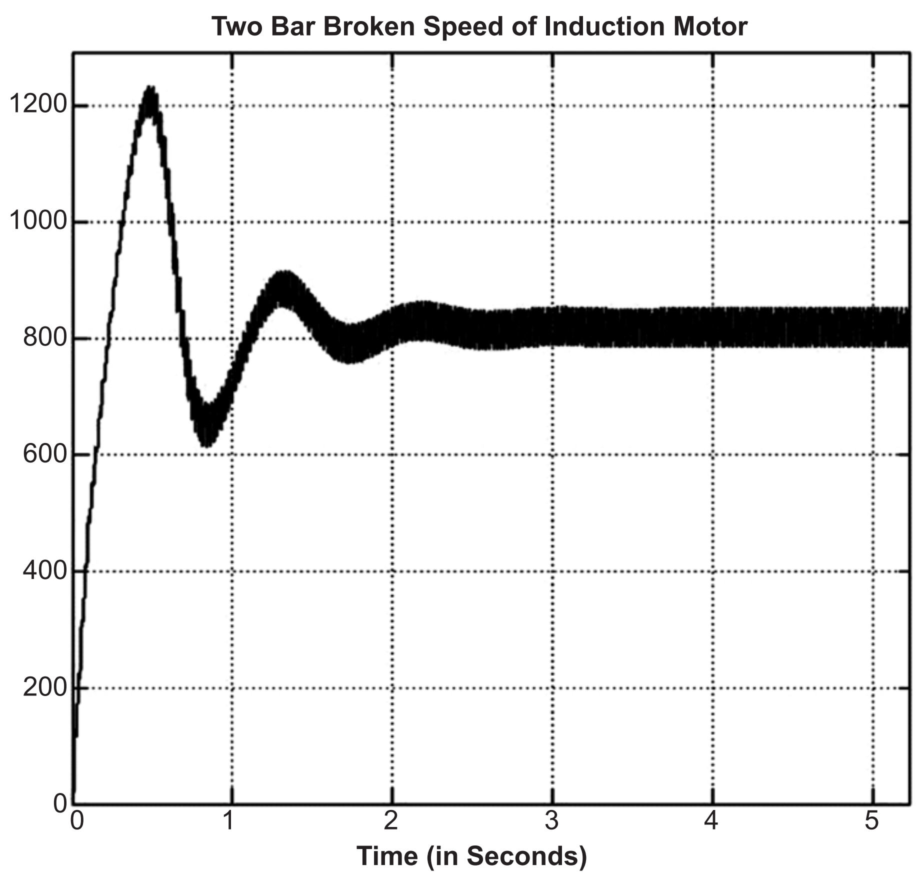

Figure 12: Two bar broken speed of induction motor

The speed and torque of healthy, one bar broken and two bar broken of induction motor is shown in the Figure 7 to Figure 12 respectively. With these waveforms, it is difficult to clearly find the difference between the healthy motor, one bar broken and two bar broken motor as the difference in speed is less for the above conditions.

Therefore to get the clear distinction of these three states of induction motor, induction motor model is simulated with wavelet tool and Park's vector approach and the simulated results are compared for the healthy motor, one broken bar and two broken bar fault.

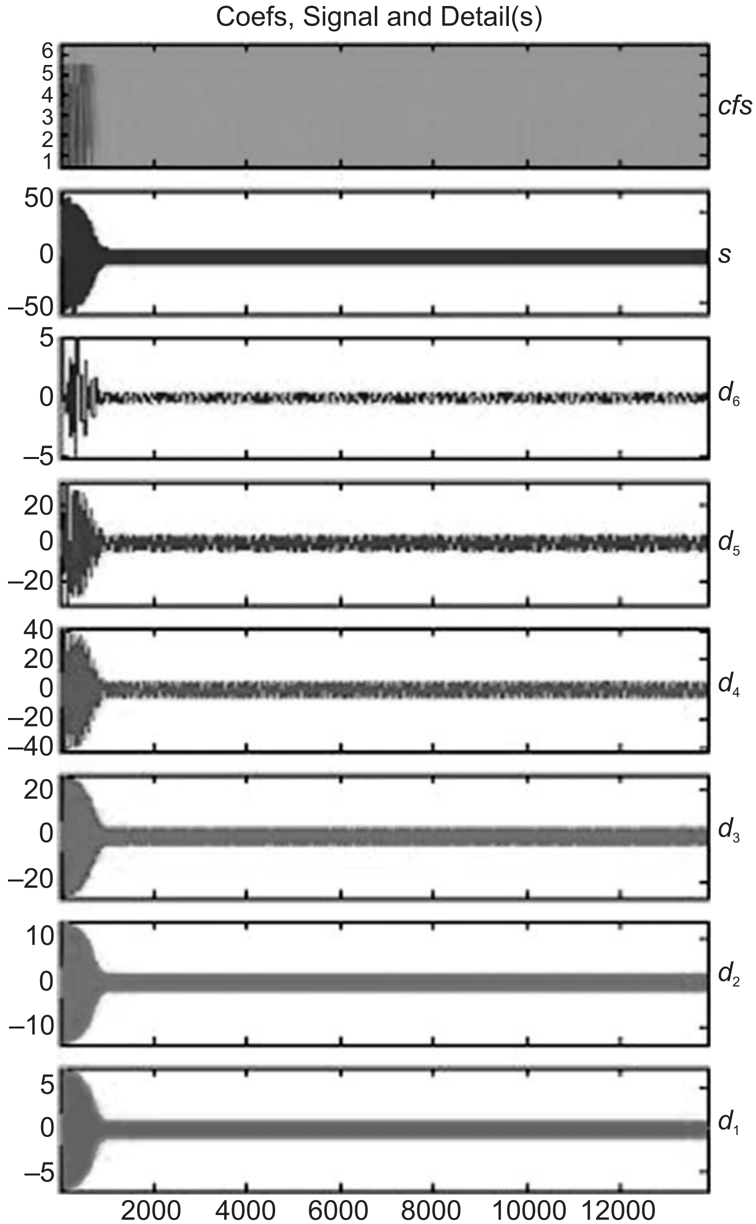

Figure 13: Healthy motor details coefficients

It is clearly evident from Figure 13 that the healthy induction motor gives lesser magnitude ripples at the sixth detail co-efficient whereas magnitude of sixth detail co-efficient shown in Figure 15 is higher, which represent the one bar broken fault, than the healthy motor sixth detail co-efficient. Park's current vector approach for Healthy motor is shown in Figure 14. Sixth detail co-efficient ripple magnitude for the two broken bar induction motor is still more, as represented in Figure 17, than the sixth detail co-efficient of healthy and one broken bar induction motor. Park's current vector approach for two bar broken induction motor is shown in Figure 18. Park's current vector approach for one bar broken induction motor is shown in Figure 16.

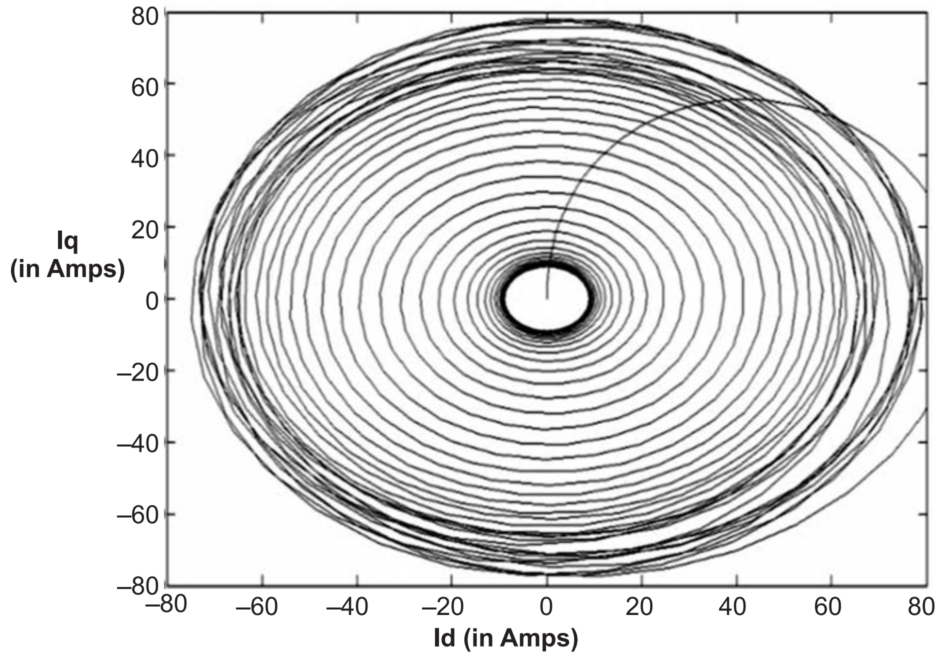

Figure 14: Park's current vector approach for Healthy motor

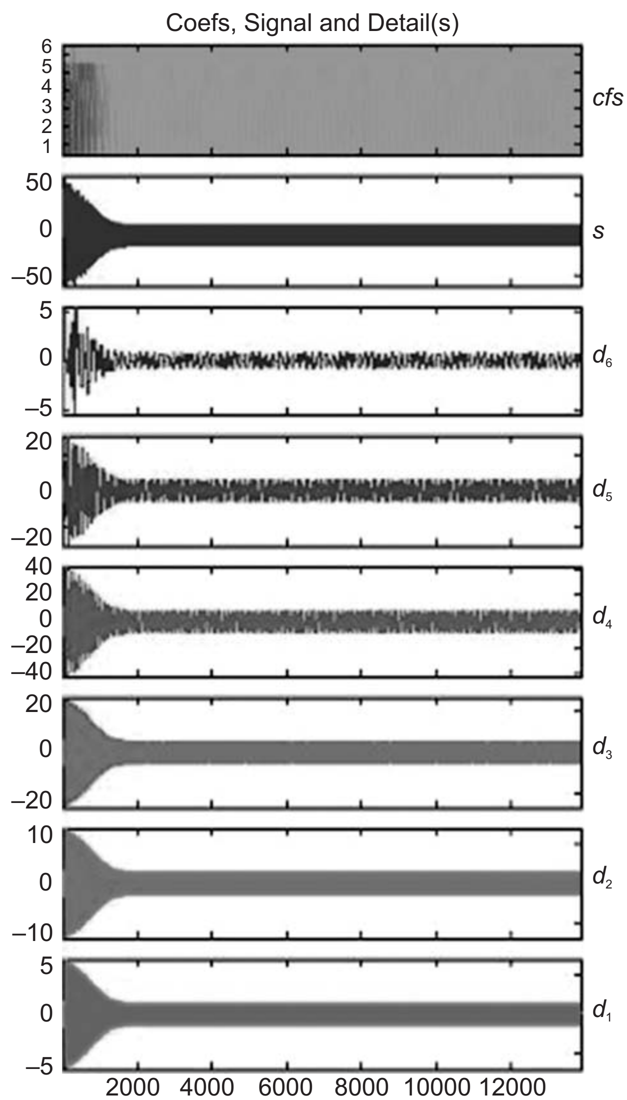

Figure 15 : One bar broken details coefficients

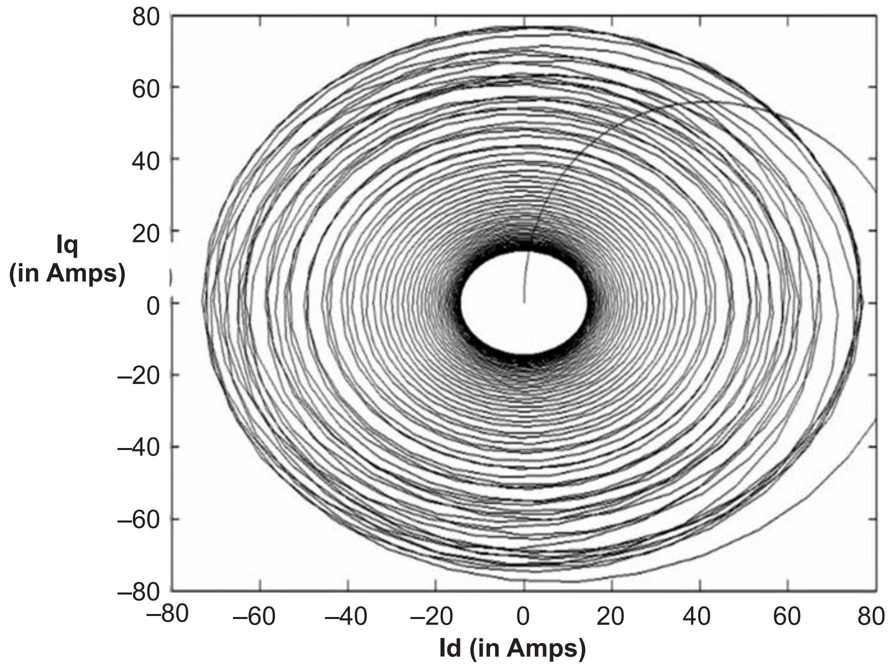

Figure 16 :Park's current vector approach for one bar broken induction motor

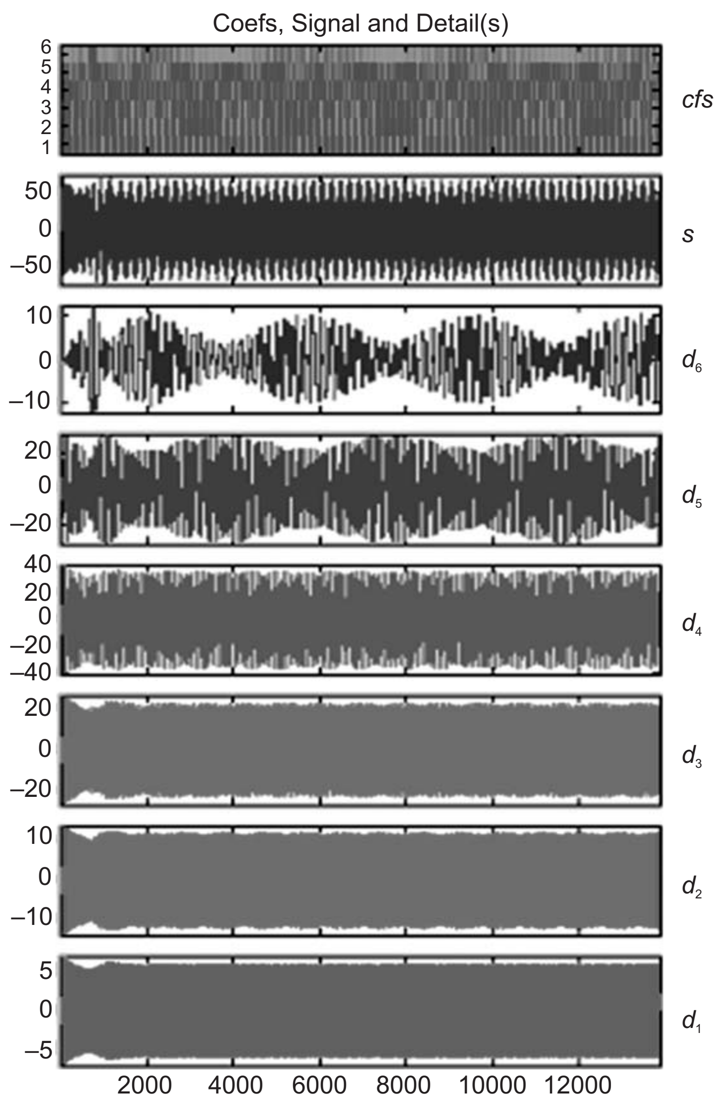

Figure 17: Two bar broken details coefficients

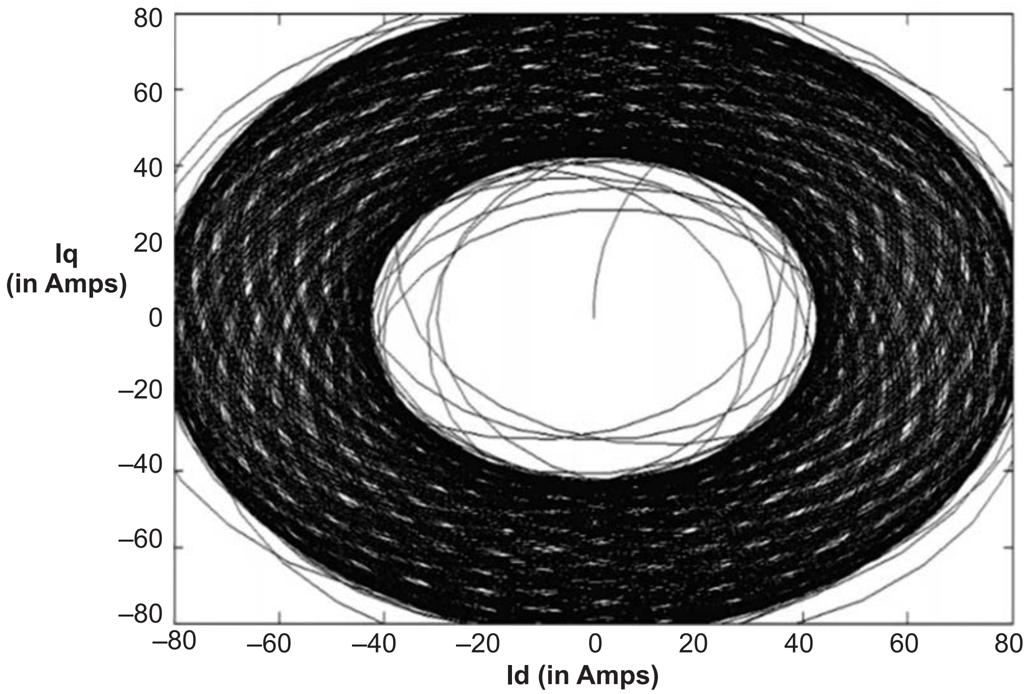

Figure 18: Park's current vector approach for two bar broken induction motor

Input voltage, V_m = 400 V

Frequency = 50 Hz

Table1
Park's Vector Values Under Healthy and Fault Conditions

3 phase induction motor condition	*Id min. (A)*	*Id max. (A)*	*Iq min. (A)*	*Iq max. (A)*
Healthy	–6.346	6.346	–6.494	6.493
One bar broken	–15.5	15.5	–9.498	9.498
Two bar	–41.46	41.46	–25.04	25.04

Park's vector pattern is plotted between the two currents I_d and I_q considering I_d in the X axis and I_q in the Y axis. Steady state value of I_d and I_q are less for the healthy induction motor, shown in Fig. 14, and steady state value of I_d and I_q gets increased as the number broken bar in the induction motor is increased. Park's vector under healthy and fault conditions are shown in Table 1.

Appendix

Induction Motor parameters :

V = 400 V
P = 4 KW
T_l = 2 Nm
R_s = 1.0405 ohm
L_s = 0.178039 H
R_r = 1.395 ohm
L_r = 0.178039 H
J = 0.013
L_m = 0.1722 H
P = 2
N = 40 (rotor bars)

6. CONCLUSION

Induction motor under healthy condition has been modeled and simulated; Single broken rotor bar and double broken rotor bar conditions of three phase induction motor have also been modeled and simulated MATLAB/SIMULNK. Induction motor stator currents, torque and speed of healthy motor and faulty motors have been displayed. Stator current of healthy and fault motors are analyzed by using wavelet daudechies 6-level decomposition technique and park's current vector approach. These analyses show the difference between healthy, single and double broken rotor bars of induction motor.

7. REFERENCES

1. A. Abed, F. Weinachter, H. Razik, A. Rezzoug. Real-time implementation of the sliding DFT applied to on-line's broken bars diagnostic. *IEEE International Conference on Electric Machines and Drives (IEMDC)*, 2001, 345-348.
2. A. Bellini, F. Filippetti, F. Franceschini, C. Tassoni, R. Passaglia, M. Saottini, G. Tontini, M. Giovannini, A. Rossi. ENEL's experience with on-line diagnosis of large induction motors cage failures. *Proc. of IEEE Industry Applications Conference*, 2000, 492-498.
3. Mohamed El Hachemi Benbouzid. A Review of induction motors signature analysis as a medium for faults detection. *IEEE transactions on industrial electronics.* 2000 October; 47(5), 984 – 993.
4. A. Bellini, F. Filippetti, F. Franceschini, T. J. Sobczyk, C. Tassoni. Diagnosis of induction machines by d-q and i.s.c. rotor models. *Proc. of IEEE SDEMPED 2005, Vienna, Austria,* 2005, 41-46.
5. C. Bruzzese, O. Honorati, E. Santini. Laboratory prototype for induction motor bar breakages experimentation and bar current measuring. *Proc. of SPEEDAM '06, Taormina, Italy*, 2006, 72-80.
6. M'hamed Drif and A.J. Marques Cardoso. The use of the instantaneous reactive power signature analysis for rotor cage fault diagnostics in three phase induction motors. *IEEE transactions on industrial electronics.* 2009 November; 56(11), 265-274.
7. C. Bruzzese, C. Boccaletti, O. Honorati, E. Santini. Rotor bars breakage in railway traction squirrel cage induction motors and diagnosis by MCSA technique. Part II: Theoretical arrangements for fault-related current sidebands. *IEEE SDEMPED 2005, Vienna, Austria*, 2005, 209-214.
8. C. Bruzzese, O. Honorati, E. Santini. Real behavior of induction motor bar breakage indicators and mathematical model. *Proc. of the ICEM 2006 Conference, Crete Island, Greece,* 2006, 111-119.
9. L. Eren and M. J. Devaney. Bearing damage detection via wavelet packet decomposition of the stator current. *IEEE Trans. Instrum. Measurements.* 2004 April; 53(2), 431–436.
10. M.E.H. Benbouzid and G. B. Kliman. What stator current processing- based technique to use for induction motor rotor faults diagnosis?. *IEEE Trans. Energy Conversion.* 2003 June; 18(2), 238-244.
11. F. Filippetti, G. Franceschini, C. Tassoni, P. Vas. AI techniques in induction machines diagnosis including the speed ripple effect. *IEEE Transactions on Industry Applications.* 1998 January/February; 34(1), 326-332.
12. S.F. Legowski, A. H. M. Sadrul Ula, A. M. Trzynadlowski. Instantaneous power as a medium for the signature analysis of induction motors. *IEEE Transactions on Industry Applications.* 1996 July/August; 32(4), 904-909.
13. B. Mirafzal, N. A. O. Demerdash. Effects of load on diagnosing broken bar faults in induction motors using the pendulous oscillation of the rotor magnetic field orientation. *Proc. of Industry Applications Conference 2004, 39th IAS Annual Meeting,* 2004, 699–707.
14. T.J. Sobczyk, W. Maciolek. Diagnostics of rotor-cage faults supported by effects due to higher MMF harmonics. *2003 IEEE PowerTech Conference, Bologna, Italy,* 2003, 110-118.
15. T.J. Sobczyk, W. Maciolek. Does the component $(1\text{-}2s)f_0$ in stator currents is sufficient for detection of rotor cage faults?. *IEEE SDEMPED 2005, Vienna, Austria, 2005,* 175-179.
16. W.T. Thomson, M. Fenger. Current signature analysis to detect induction motor faults. *IEEE Industry Applications Magazine*, 2001 July/August; 7, 26-34.
17. M'hamed Drif and A.J. Marques Cardoso. Air gap eccentricity fault diagnosis, in three phase induction motors, by the complex apparent power signature analysis. *IEEE transactions on industrial electronics.* 2008 March; 55(3), 1404-1410.
18. Xia Ying. Performance evaluation and thermal fields analysis of induction motor with broken rotor bars located at different relative positions. *IEEE transactions on magnetic.* 2010 May; 46(5), 1243 -1250.
19. Vinod V. Thomas, Krishna Vasudevan and V. Jagadeesh Kumar. On line cage rotor fault detection using air gap torque spectra. *IEEE transactions on energy conversion.* 2003 June; 18, 265-270.
20. P.Govindamoorthi, K.Valarmathi. Classification of faults in DTC induction machine using wavelet decomposition method. *Indian journal of science and technolog.* 2015 October; 8(26), 313-324.